

# Health Monitoring of Tree-Trunks Using Ground Penetrating Radar

Iraklis Giannakis, Fabio Tosti, Livia Lantini, and Amir Alani

**Abstract**—Ground penetrating radar (GPR) is traditionally applied to smooth surfaces in which the assumption of half-space is an adequate approximation that does not deviate much from reality. Nonetheless, using GPR for internal structure characterization of tree trunks requires measurements on an irregularly shaped closed curve. Typical hyperbola-fitting has no physical meaning in this new context since the reflection patterns are strongly associated to the shape of the tree trunk. Instead of a clinical hyperbola, the reflections give rise to complex-shaped patterns that are difficult to be analyzed even in the absence of clutter. In the current paper, a novel processing scheme is described that can interpret complex reflection patterns assuming a circular target subject to any arbitrary shaped surface. The proposed methodology can be applied using commercial hand-held antennas in real-time avoiding computationally costly tomographic approaches that require the usage of custom-made bespoke antenna arrays. The validity of the current approach is illustrated both with numerical and real experiments.

**Index Terms**—GPR, hyperbola fitting, Tree, Trunk.

## I. INTRODUCTION

Monitoring wood materials is of great importance with both industrial and environmental applications [1], [2]. Preserving cultural-heritage objects [1], evaluating the structural stability of wooden-based structures [1] and assessing the health conditions of living trees [3] are amongst the areas in which wood imaging has been successfully applied. A direct method for monitoring the internal structure of the wood is core-drilling [4]. This is a time-consuming intrusive methodology that can potentially damage the tree. To that extend, non-destructive testing (NDT) has been suggested in an effort to provide a reliable and a non-intrusive scheme for estimating the internal structure of wood.

NDT utilizes received information in an effort to indirectly map the physical properties of the tree trunk. Amongst the investigated properties are the water content, the dielectric properties, the elastic properties and the density [1]. From the investigated properties it is apparent that a wide range of NDT and geophysical methods need to be applied, from estimating the elasticity of the wood by mechanical means [5], minimum intrusive techniques like drilling resistance [6] and electrical resistivity tomography (ERT) [7], [8] to ultrasound tomography [9], thermography [10], [11], [12] and more sophisticated techniques like X-ray computed tomography (CT-scan) [13] and neutron imaging [14], [15]. These techniques differ with respect to accuracy, limitations and practicality. For example, CT-scan can provide a very accurate and detailed

image of the internal structure of the tree, nonetheless, when field measurements and fast results are required, CT-scan is neither attainable nor commercially appealing.

A particularly challenging application of wood monitoring is assessing the health condition of living trees [3]. Monitoring living trees has some inherited constraints arising from the nature of the acquisition. Any methodology proposed to tackle this problem should have reasonable computational requirements in order to be applicable in large scale projects like forestry applications. In addition, detecting tree decays requires extensive field measurements in non-trivial environments. Therefore, any equipment necessary for the acquisitions should be portable and easily deployable to the site of interest. In that context, ground penetrating radar (GPR) has been suggested as a potential methodology to assess the health conditions of trees in a reliable and efficient manner [3], [16].

Due to the cylindrical shape of the trees, tomographic approaches are particularly appealing from a mathematical point of view. Microwave imaging of cylindrical bodies has been widely applied for biomedical applications [17] using inversion schemes primarily based on linear approximations [21], [20]. This framework has been extrapolated for assessing the internal structure of tree trunks with promising results [19]. In the same context, Ray-based tomography using GPR has also been tested for detecting anomalies inside tree-trunks [18]. To our knowledge, full waveform inversion (FWI) applied on tree monitoring has not been reported to the literature. FWI is a powerful tool for interpreting GPR data [22], [23], [24], nonetheless, its high computational requirements combined with the need for an accurate antenna model incorporated in the forward solver [25] make implementation of FWI to GPR a laborious process with limited commercial applications.

Tomographic approaches, apart from being computationally demanding, they also require a full set of measurements with multiple transmitters and receivers often using custom-made bespoke systems [19]. This deviates from the norm since GPR surveys traditionally employ commercial antennas using the common-offset method of measurements [26]. In that context, in an effort to develop a commercially appealing methodology, a signal processing approach is presented in the current paper that estimates the size and the coordinates of tree decays using common-offset commercial systems.

Circular targets subject to a homogeneous half-space give rise to hyperbolic features in the measured B-Scans. Hyperbola fitting is a mainstream processing approach in the GPR community [26] due to its simplicity and effectiveness when the assumptions are met. Hyperbola-fitting can be interpreted as a typical minimization of distance between given points and a hyperbola [27]. Nonetheless, due to the noise and the

Iraklis Giannakis, Livia Lantini, Fabio Tosti and Amir Alani are with the school of computing and engineering, University of West London, London, W5 5RF, iraklis.giannakis@uwl.ac.uk, fabio.tosti@uwl.ac.uk, livia.lantini@uwl.ac.uk, amir.alani@uwl.ac.uk.

clutter inherently present in B-Scans, an automatic hyperbola fitting is a challenging task that often requires pre-processing prior to any fitting scheme [28], [29]. In addition, similar hyperbolic patterns can emerge for different sets of target's radii and permittivity values, introducing non-uniqueness to the problem [28]. Knowing the velocity of the medium, or assuming a point-target, Hough transform for hyperbolas can be utilized in an effort to map the distribution of the hyperbolas on a given B-Scan [26], [30], [31]. Hough transform can be seen as a brute force optimization that maps the given feature space and subsequently detects local minimal which are identified as hyperbolas. The brute-force nature of Hough transform makes this approach computationally demanding with a computational burden that expands geometrically when the resolution of the feature space is increased [29]. One of the most effective methods to reduce the feature space is to apply machine learning prior to Hough transform in order to detect sub-spaces that contain hyperbolas [32]. In [33], a Viola-Jones [34] detection scheme is applied in order to automatically detect areas in which hyperbolas are present. As it is stated in [29], the training process requires an extensive library of both positive and negative B-Scans in order for the classifier to be sufficiently trained.

All the methods mentioned above focus on circular targets buried in a homogeneous half-space. Evaluating the internal structure of cylindrical targets –like tree trunks– requires a more generic approach, since the assumption of half-space is no longer valid. Tree trunks are complicated structures and their shape differs based on age, species and environmental conditions [35]. The proposed scheme expands the traditional hyperbola fitting method [28], [29] from half-spaces to arbitrary complex shapes. Prior to that, a practical positioning approach should be established. Commercial GPR systems use a wheel-based system in order to associate each A-Scan with a specific distance from a given reference point. A wheel-based system of positioning is very practical when applied to line measurements. Nonetheless, plane measurements on irregular surfaces require a transformation of distance to 2D coordinates. To that extend, an arc length approach is presented which can be applied in any plane measurements using wheel-based positioning system.

Subsequently, image processing is applied in an effort to remove the ringing noise present in the B-Scans due to the layers of the tree. In this paper two approaches have been chosen based on their performance and computational simplicity. The first one is the singular value decomposition (SVD) filter [36], [37] and the second one is the linear combination filter [38]. The image is then manually thresholded [45], [29] and a particle-swarm optimization (PSO) is used to fit the resulting anomaly, which can no longer be approximated with a hyperbola. Global optimizers like PSO [39] overcome local minimal and make any initialization scheme unnecessary. Global optimizers can be seen as an intermediate step between convex non-linear least squares fitting [27] and brute force approaches like Hough transform [30], [31]. Hence, PSO balances between efficiency and accuracy.

The suggested scheme has been successfully tested using commercial antennas in both synthetic and real data. This

supports the premise that the proposed methodology is a reliable approach with minimum computational and operational requirements that can be applied in a straightforward manner to large scale forestry applications.

## II. REFLECTION PATTERNS USING COMMON OFFSET CONFIGURATION

Typical GPR surveys take place in flat surfaces along a straight line. Each A-Scan is associated with a given position on that line based on the distance measured from a reference point. This distance is measured using a wheel-measuring device which is often incorporated in commercial GPR transducers. It is apparent that when the survey takes place in a straight line, distance can be trivially associated with a unique ordinate. This is not the case when the measurements are taken on irregular surfaces such as tree trunks. This problem is known as arc length parametrization and has a wide range of applications to computer graphics [40], [41].

### A. Transforming Distance to Coordinates

In this section an inclusive scheme based on [41] is described that can be applied in any arbitrary shaped host medium. Initially, the shape of interest is defined in  $x, y$  coordinates  $\{x, y \in \mathbb{R} \mid x, y > 0\}$  discretized with an arbitrary non-uniform discretization step. The coordinates  $x, y$  are stored into the vectors  $\mathbf{x} \in \mathbb{R}^n$  and  $\mathbf{y} \in \mathbb{R}^n$  respectively, where  $n$  is the number of points used to discretise the shape of the host medium. The vector  $\mathbf{t} = \langle t_1, t_2, \dots, t_n \rangle \{t \in \mathbb{R}^n \mid 0 \leq t_i \leq 1\}$  is then defined which is going to be used as the arbitrary variable for the parametric representation of the shape of the host medium. The components of  $\mathbf{t}$  increase linearly from zero to one with a constant step  $\frac{1}{n}$ , i.e.  $\mathbf{t} = \langle 0, \frac{1}{n}, \frac{2}{n}, \dots, 1 \rangle$ . Using spline interpolation for the vectors  $(\mathbf{y}, \mathbf{t})$ , a set of polynomial functions are obtained. The latter, map  $y$  to  $t$  in a continuous manner.

$$P_i : [t_i, t_{i+1}] \rightarrow \mathbb{R} \quad (1)$$

Similarly, spline interpolation is used to map  $x$  with respect to  $t$

$$Q_i : [t_i, t_{i+1}] \rightarrow \mathbb{R} \quad (2)$$

Each of the functions  $P_i, Q_i$  are polynomials of the third order

$$P_i(t) = A_{p,i}t^3 + B_{p,i}t^2 + C_{p,i}t + D_{p,i}, \quad \forall t \in [t_i, t_{i+1}] \quad (3)$$

$$Q_i(t) = A_{q,i}t^3 + B_{q,i}t^2 + C_{q,i}t + D_{q,i}, \quad \forall t \in [t_i, t_{i+1}] \quad (4)$$

Therefore, an arbitrary complex shape defined through discretized measurements can now be expressed in a vector form as  $\mathbf{F} = \langle P(t), Q(t) \rangle$ . The shape can now be mapped with an arbitrary step since both  $x$  and  $y$  are expressed in a continuous manner.

The arc length of a planar curve in  $\mathbb{R}^2$  written in a vector form  $\mathbf{F} \{\mathbf{F} \in \mathbb{R}^2\}$  is evaluated by [42]

$$s(\tau) = \int_0^\tau \left\| \frac{d\mathbf{F}}{dt} \right\| dt = \int_0^\tau \sqrt{\left( \frac{dP(t)}{dt} \right)^2 + \left( \frac{dQ(t)}{dt} \right)^2} dt \quad (5)$$

where

$$\frac{dP_i(t)}{dt} = 3A_{p,i}t^2 + 2B_{p,i}t + C_{p,i}, \quad \forall t \in [t_i, t_{i+1}] \quad (6)$$

$$\frac{dQ_i(t)}{dt} = 3A_{q,i}t^2 + 2B_{q,i}t + C_{q,i}, \quad \forall t \in [t_i, t_{i+1}] \quad (7)$$

Arc length (5) has analytical solutions for limited number of curves (circle, catenary function etc.). For complicated shapes such as tree-trunks, the integral in (5) can be approximated numerically by

$$s(N\Delta t) \approx \sum_{k=0}^N \left\| \frac{d\langle P(k\Delta t), Q(k\Delta t) \rangle}{dt} \right\| \Delta t \quad (8)$$

where  $\Delta t = \frac{\tau}{N}$ . From (8) it is evident that

$$s(N\Delta t) \approx s((N-1)\Delta t) + \left\| \frac{d\langle P(N\Delta t), Q(N\Delta t) \rangle}{dt} \right\| \Delta t \quad (9)$$

Equation (9) is an efficient way to compute  $s(\tau)$  from its previous values without having to evaluate the summation in (8) for every time step. Using a spline interpolation, the values of  $\tau$  can be mapped with respect to  $s$  in a continuous manner

$$T_i : [s_i, s_{i+1}] \rightarrow \mathbb{R} \quad (10)$$

The function  $T(s)$  approximates the value of the parameter  $\tau$  with respect to the length  $s$ . Thus, for a given distance  $s$  the parametric variable  $\tau$  associated with this distance can be estimated. Consequently, the positional vector  $\mathbf{F} = \langle P(T(s)), Q(T(s)) \rangle$  can now be connected to a given distance  $s$ . In that way, the distance measured by the wheel-measuring devices in commercial GPR antennas can be transformed to  $x, y$  coordinates using a limited amount of points to discretise the curve of interest.

### B. Reflection-Arrival Travel-Time

The reflection-arrival travel-time is related to the distance –relative to a reference point– of each measurement via a hyperbolic equation [28]. The interpretation of the resulting hyperbola gives us an insight on the burial-depth of the target, the velocity of the host medium and the size of the target [28]. The above holds true when the assumptions are met i.e. when the host medium has a flat surface, when the target is circular and when the host medium is homogeneous. When the investigated surface is not flat, the resulting reflection patterns can no longer be approximated with a hyperbola [43], [44]. In [43] and [44] the reflection patterns that occur when the host medium is a cylinder are investigated and analyzed in detail. The scheme presented by [43] and [44] can be expanded to any arbitrary shape via

$$t(s) = \left( \left\| \mathbf{F}(s) - \langle x_g, y_g \rangle \right\| - R \right) \frac{\sqrt{\epsilon}}{c_0} \quad (11)$$

where  $t$  is time (seconds),  $\mathbf{F}(s) = \langle x_s, y_s \rangle$  is the positional vector (meters) along the surface of the tree with respect to the distance from a reference point (see II.A),  $R$  is the radius of the cylindrical target (meters),  $\epsilon$  is the relative permittivity of the host medium,  $c_0$  is the speed of light ( $c_0 \approx 3 \cdot 10^8$ , m/s) and  $\langle x_g, y_g \rangle$  are the coordinates of the center of the target

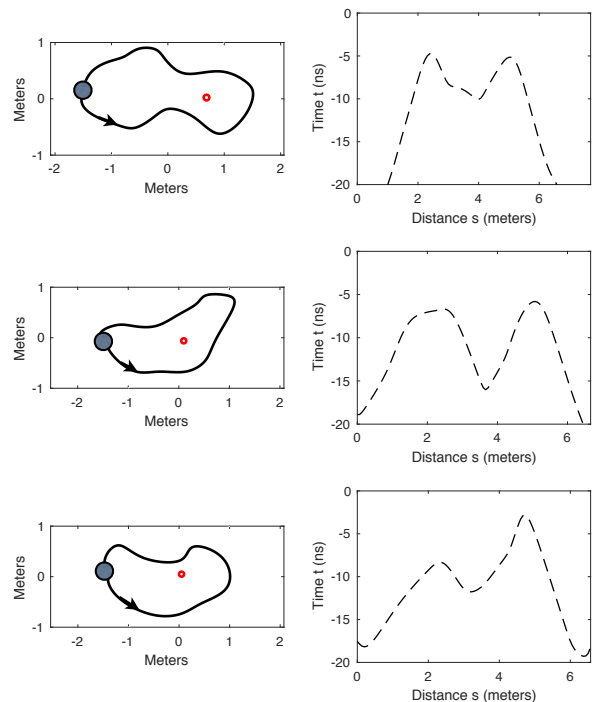


Fig. 1. Left: With black line is the shape of the host medium. The gray circles indicate the starting points of the measurements. The direction of the measurements is counter-clockwise. Red circles indicate the targets of interest. Right: The arrival travel-time from the target is plotted with respect to the distance relative to the starting point (11).

(meters). As it is shown in Fig. 1, the relationship between  $s$  and  $t$  (11) for realistic tree trunks is complicated and highly related to the shape of the tree.

## III. PROCESSING FRAMEWORK

The processing framework proposed in this paper consists of two parts. Initially an SVD [36] and a linear filter [38] are used in order to reduce the ringing noise that is present to the measured B-Scans due to the layered nature of the tree-trunk [35]. The post-processed data are then manually thresholded and a PSO is used in order to estimate the origins and the size of the targets based on their reflection patterns.

### A. Ringing noise removal

A generic tree-trunk consists of five distinct layers, namely, bark, phloem, cambium, heartwood and sapwood [35]. The aforementioned layers differ with respect to water content as well as chemical composition and texture [35]. This results to dielectric contrasts that give rise to repetitive reflections contributing to the overall ringing noise. Due to that, two different methodologies are employed in an effort to reduce ringing noise and increase the overall signal to clutter ratio.

The data are collected along a given curve and each A-Scan  $\mathbf{A}_s \in \mathbb{R}^w$  is a vector with size  $w$  which is measured at distance  $s$  from the starting point. The B-Scan  $\mathbf{B} \in \mathbb{R}^{w \times S}$  is a 2D matrix with  $w \times S$  dimensions where  $S$  is the number of measurements and  $\mathbf{B} = \langle \mathbf{A}_{s_1}^T, \mathbf{A}_{s_2}^T, \dots, \mathbf{A}_{s_w}^T \rangle$  ( $T$  denotes the transpose sign). Ringing noise shows similar behavior between

A-Scans [45], [46]. This is the reason why a simple average removal [26] can often efficiently decrease ringing noise. Nonetheless, as it is stated in [36], other approaches like SVD provide a more accurate and systematic way to reduce ringing noise in challenging scenarios with low signal to clutter ratio.

In SVD, the matrix  $\mathbf{B}$  is decomposed into three matrices [36]

$$\mathbf{B} = \mathbf{U}\mathbf{M}\mathbf{V}^T \quad (12)$$

where  $\mathbf{U} \in \mathbb{R}^{w \times w}$  and  $\mathbf{V} \in \mathbb{R}^{S \times S}$  are orthogonal matrices and  $\mathbf{M} \in \mathbb{R}^{w \times S}$  is a diagonal matrix that contains the eigenvalues of  $\mathbf{B}$  arranged in a decreasing order. The large eigenvalues are associated with dominant repetitive features most often associated with ringing noise while small eigenvalues represent uncorrelated features like clutter and noise [47]. A typical SVD filter keeps the intermediate eigenvalues while setting the rest to zero

$$\bar{\mathbf{B}} = \bar{\mathbf{U}}\bar{\mathbf{M}}\bar{\mathbf{V}}^T \quad (13)$$

where  $\bar{\mathbf{M}} \in \mathbb{R}^{w \times S}$ ,  $\{\bar{\mathbf{M}}_{i,i} = 0 \mid \forall i [m_1, m_2]\}$  and  $m_1$  and  $m_2$  are the lower and upper eigenvalue-boundaries for the SVD filter.

SVD is a powerful tool for removing ringing noise, nonetheless as it is stated in [37], the performance of processing frameworks are case dependent and there is no conclusive approach that over-performs the rest. To that extend, a linear approximation of the signal is also considered as an alternative to SVD [47], [38]. The linear approximation uses a matrix  $\mathbf{J} \in \mathbb{R}^{w \times q}$  that contains  $q$  number of randomly selected traces without the present of any target. Subsequently, it is assumed, that any A-Scan consists of the target's response ( $\mathbf{E}_s$ ) plus clutter ( $\mathbf{E}_c$ )

$$\mathbf{A}_i = \mathbf{E}_{i,c} + \mathbf{E}_{i,s} \quad (14)$$

The term clutter here is used to describe ringing noise, noise and the cross-coupling between the transmitter and the receiver. Approximating  $\mathbf{A}_i$  as a linear combination of the traces in  $\mathbf{J}$ , will result to a sufficient approximation of  $\mathbf{E}_c$  and a poor approximation of  $\mathbf{E}_s$ . This is due to the fact that the clutter is correlated between the traces and it is easier to be modeled based on previous A-Scans. Using least squares, the linear coefficients of the matrix  $\mathbf{J}$  are evaluated and subsequently the predicted clutter is subtracted from each A-Scan

$$\bar{\mathbf{A}}_i^T = \mathbf{A}_i^T - \mathbf{J}(\mathbf{J}^T\mathbf{J})^{-1}\mathbf{J}^T\mathbf{A}_i^T \quad (15)$$

### B. Model Fitting

The current subsection presents the equivalent of "hyperbola-fitting" to the more inclusive and generic reflection patterns that are expected in tree-trunks. Through a manual threshold, the anomaly of interest can be gathered in a set of points  $M = \{(s_i, t_i) \in \mathbb{R}, |i = 1, 2, \dots, z\}$ , where  $z$  is the number of observations. Based on  $M$  and (11), the center  $\langle x_g, y_g \rangle$  of the target, its radius  $R$  and the relative permittivity of the host medium  $\epsilon$  are fine tuned in order to minimize

$$\operatorname{argmin}_{x_g, y_g, \epsilon, R} \sum_{i=1}^z \left( t_i - (\|\mathbf{F}(s_i) - \langle x_g, y_g \rangle\| - R) \frac{\sqrt{\epsilon}}{c_0} \right)^2 \quad (16)$$

It is easy to show that (16) can be re-written as

$$\operatorname{argmin}_{x_g, y_g, \epsilon, R} \sum_{i=1}^z \left( t_i - \|\mathbf{F}(s_i) - \langle x_g, y_g \rangle\| \frac{\sqrt{\epsilon}}{c_0} + R \frac{\sqrt{\epsilon}}{c_0} \right)^2 \quad (17)$$

From (17), it is apparent that the radius  $R$  and the relative permittivity  $\epsilon$  form a non-unique product. That means that different sets of  $(R, \epsilon)$  might result to similar outputs. Thus, in the presence of noise, the minimization in (17) is sensitive due to non-uniqueness. This phenomenon was derived experimentally in [28] for flat surface surveys.

To overcome this, the bulk relative permittivity of the tree trunk can be approximated using the two-way travel-time from the reflection of the opposite side of the tree. Knowing the time needed for the electromagnetic wave to travel a known distance, the mean relative permittivity can be evaluated in a straightforward manner. If the relative permittivity is not readily available, then the minimization in (17) can be executed subject to a idealized point target i.e. for  $R = 0$ .

The function to be minimized in (17) is subject to multiple local minimal due to the nature of the problem as well as the inherited noise in the measured  $M$ . To avoid initialization and overcome local minimal, a global optimizer is used for executing (17). For the current paper, PSO [39] is chosen due to its popularity in electromagnetics [48], [49] and geophysics [50]. Using a different global optimizer (i.e. genetic algorithms, ant colony optimization etc.) will have minor differences on the overall performance and computational requirements of the detection scheme. PSO initially generates a number of particles  $u$  that are placed randomly in the optimization space. For the case that permittivity is known, each particle  $k$  is a vector  $\mathbf{q}_k = \langle x_k, y_k, R_k \rangle \{\mathbf{q}_k \in \mathbb{R}^3\}$ . The cost function is then evaluated for every particle and their positions are updated in an iterative manner

$$\mathbf{v}_k^\tau = b_0 \mathbf{v}_k^{\tau-1} + b_1 V_1 (\mathbf{q}_k^{\tau-1} - \mathbf{q}_{k,b}) + b_2 V_2 (\mathbf{q}_k^{\tau-1} - \mathbf{q}_g) \quad (18)$$

$$\mathbf{q}_k^\tau = \mathbf{q}_k^{\tau-1} + \mathbf{v}_k^\tau$$

where  $b_0$ ,  $b_1$  and  $b_2$  are constants associated with the convergence rate and the ability of PSO to converge to global solutions. In general, large values of  $b_0$  and small values of  $b_2$  decrease the convergence rate and the probability of the algorithm to be trapped in local minimal. The parameters  $V_1, V_2 \in [0, 1]$  are random numbers with a uniform distribution and  $\tau \in \mathbb{Z}$  is the integer iteration number. The vector  $\mathbf{v}_k \in \mathbb{R}^3$  is the velocity in the three dimensions of  $\mathbf{q}_k$ . The vector  $\mathbf{q}_{k,b}$  is the position  $\langle x_k, y_k, R_k \rangle$  of the particle  $k$  in which the cost function got its minimum value until the iteration  $\tau$ . Lastly the vector  $\mathbf{q}_g$  is the position  $\langle x, y, R \rangle$  in which the cost function from all the particles got its minimum value until the iteration  $\tau$ . For the current case –through trial and error– it is derived that  $u = 50$  and  $b_0 = b_1 = b_2 = 1$  balances between efficiency and accuracy.

## IV. NUMERICAL EXPERIMENTS

In the current section, the proposed methodology is tested on synthetic data. A second order in both space and time finite-differences time-domain (FDTD) [51] method is used

TABLE I  
THE EXTENDED DEBYE PROPERTIES OF THE TREE LAYERS

Name	WC	$\epsilon_\infty$	$\Delta\epsilon$	$\sigma$ ( $\Omega^{-1}m^{-1}$ )	$t_0$ (sec)
Cabdiium layer	40 %	6	18	1	9.23e-12
Outer Sapwood	30 %	6.1	12.36	0.033	9.23e-12
Inner Sapwood	25 %	5.9	9.66	0.02	9.23e-12
Rings	10 %	5.4	3.1	0.0083	9.23e-12
Heartwood	5 %	5.22	1.43	0.005	9.23e-12
Bark	0 %	5	0	0	9.23e-12

in order to numerically evaluate Maxwell's equations for a given dielectric distribution. In an effort to accelerate the computations, gprMax [53], an open-source CUDA-based GPU engine [52] is employed. The spatial discretization step is assumed to be uniform throughout the grid and equal with  $\Delta x = \Delta y = \Delta z = 0.001$  m. The time step  $\Delta t$  follows the Courant limit [51].

The dielectric properties of wood vary seasonally as well as with respect to the type of the tree [54]. In general, softwoods contain more water content compared to hardwoods. Consequently, the permittivity of softwoods is substantially higher than the one of hardwoods [54]. The permittivity is also related to the orientation of measurement, i.e. the tree-trunk is an anisotropic material, with the lowest permittivity values observed perpendicular to the layering of the tree [54]. A typical tree-trunk consists of five layers, namely, the bark, the phlem, the cabdiium cell layer, the outer and inner sapwood and the heartwood [35]. In addition to these layers, thinner rings of dense material occur in a periodic manner and almost parallel to each other [35]. The water content of the aforementioned structures greatly varies between different types of trees. For example, hardwoods consist of a dry heartwood and a saturated sapwood in contrast to softwoods for which both sapwood and hardwood are equally saturated [54]. Numerous attempts have been made to generate semi-empirical models for the dielectric properties of trees similar to the semi-empirical models that exist for soils [55]. Nonetheless, a conclusive formula is not yet to be derived due to the complexity of the tree structure and its multi-phase composition.

Experimental evidences support the premise that the permittivity of trees increases linearly with the increase of water content [56]. Electrolytes and cellulose seems to have a secondary effect [54]. Due to its water content and the bipolar nature of the latter, the relative permittivity of the tree trunk can be expressed as an extended Debye model [54], [57], [58]

$$\epsilon(\omega) = \epsilon_\infty + \frac{\Delta\epsilon}{1 + j\omega t_0} - \frac{\sigma}{j\omega\epsilon_0} \quad (19)$$

where  $j = \sqrt{-1}$ ,  $\epsilon$  is the relative permittivity of the material with respect to  $\omega$ ,  $\omega$  is the angular frequency,  $\epsilon_\infty$  is the relative permittivity at infinity frequency,  $\Delta\epsilon$  is the difference between the static relative permittivity and the relative permittivity at infinity frequency,  $t_0$  is the relaxation time and  $\sigma$  is the conductive term. In order to map the underlying relationship between the dielectric parameters in (19) and the water content of the trunk, the complex refractive index model (CRIM) [59]

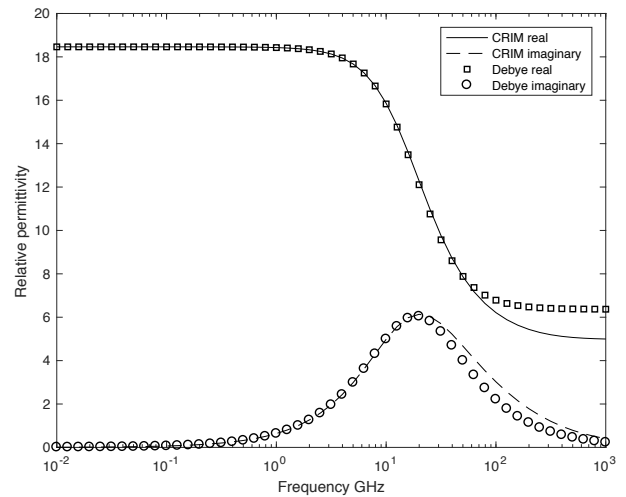


Fig. 2. Dielectric properties for the outer sapwood using CRIM model and its Debye equivalent. It is apparent that up to 10 GHz, one Debye pole is adequate for the approximation in (21).

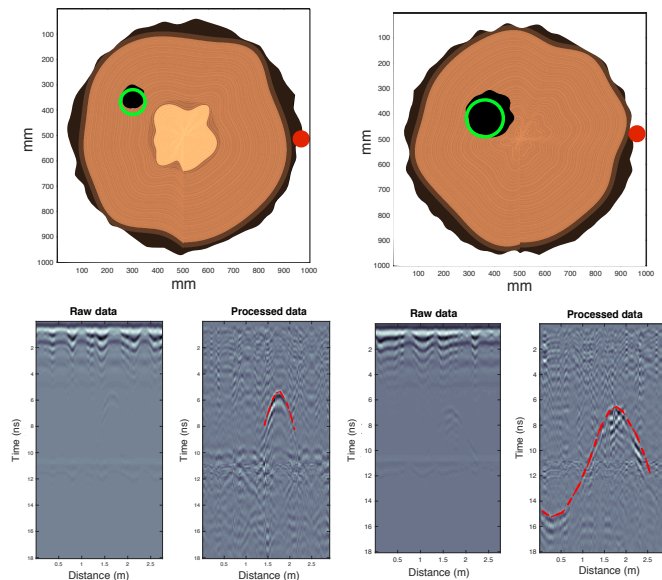


Fig. 3. One saturated hardwood (left) and one semi-saturated softwood (right) are numerically simulated. The green lines indicate the recovered tree decays using the suggested scheme. Red circles indicate the starting point. The measurements are taken clockwise.

is used. The latter, assumes that the tree-trunk is a two-phase material and its relative bulk permittivity equals with

$$\sqrt{\epsilon} = f_t \sqrt{\epsilon_t} + f_w \sqrt{\epsilon_w} \quad (20)$$

where  $\epsilon$  is the relative bulk permittivity of the material,  $\epsilon_t = 5$  is the relative permittivity of the solid phase of the tree,  $\epsilon_w = 4.9 + 78 / (1 + j\omega(9.23e - 12))$  is the dispersive relative permittivity of the water [55] and  $f_t$  and  $f_w$  are the volumetric fractions for the solid and the water phase respectively ( $f_t + f_w = 1$ ).

The CRIM model provides a simple and elegant way to express the bulk permittivity of a multi-phase medium with respect to its phases. Nonetheless, CRIM can not be imple-

mented directly to FDTD. To overcome this, equation (20) should be replaced with a function compatible with FDTD [60]. Given a specified volumetric water fraction, equation (20) can be approximated for a given frequency range  $[\omega_l, \omega_u]$  by a multi-Debye pole

$$f_t \sqrt{\epsilon_t} + f_w \sqrt{\epsilon_w} \approx \epsilon_\infty + \sum_{h=1}^H \frac{\Delta \epsilon_h}{1 + j\omega t_{0,h}}, \quad \forall \omega \in [\omega_l, \omega_u] \quad (21)$$

The approximation above can be seen as a minimization problem

$$\operatorname{argmin}_{\Delta \epsilon_h, t_{0,h}, \epsilon_\infty} \sum_{i=l}^u \left( f_t \sqrt{\epsilon_t} + f_w \sqrt{\epsilon_w} - \epsilon_\infty - \sum_{h=1}^H \frac{\Delta \epsilon_h}{1 + j\omega_i t_{0,h}} \right)^2 \quad (22)$$

The minimization in (22) is executed using the hybrid scheme proposed in [49] for approximating Havriliak-Negami media with multi-Debye expansions. From Fig 2 it is clear that one Debye pole ( $H = 1$ ) is sufficient for approximating (21) for the frequency range of 0.01–10 GHz. In the current numerical study, the water content of the tree layers are chosen such as to simulate saturated hardwoods like oaks or relatively dry softwoods like cedars. The Debye properties –derived from (22)– of the tree layers used in this numerical study are shown in Table I. The conductivities are chosen based on typical values measured using electrical resistivity tomography [61], [62].

#### A. Numerical Case Study

Hollow cavities throughout the tree trunk is a typical sign of tree decay and a robust indicator of the health status of the tree [63], [64]. Detecting cavities in a non-destructive manner is of high importance since extended cavities can compromise the stability and the structural integrity of the trunk leading to tree falls [63]. In the current numerical study, the ability of the current scheme on detecting hollow cavities is investigated in two different numerical experiments.

The first case study is shown in Fig. 3. One saturated hardwood and one semi-saturated softwood are investigated. For the saturated hardwood, the trunk consists of bark, cambium layer, outer sapwood and heartwood. In the second case, the trunk consists of bark, cambium layer and outer sapwood. For the excitation of the FDTD a numerical equivalent of the commercial antenna GSSI 1.5 GHz is used [25], [65]. **The excitation of the antenna is constrained to be parallel to one the Cartesian axes due to the arrangement of the fields in FDTD. Therefore, the models described in [25], [65] do not support tilted measurements. To overcome this, instead of rotating the antenna around the trunk, the trunk is rotated while the position of the antenna is fixed.** The resulting B-Scan is processed using an SVD filter removing the six dominant eigenvalues. From Fig. 3 it is evident that the proposed scheme can accurately recover both the size as well as the location of the decay when the permittivity is known. For the current example, a mean relative permittivity  $\epsilon = 18$  is assumed. If the permittivity is treated as an unknown in (17), the center of the target can be accurately estimated, nonetheless, its radius must

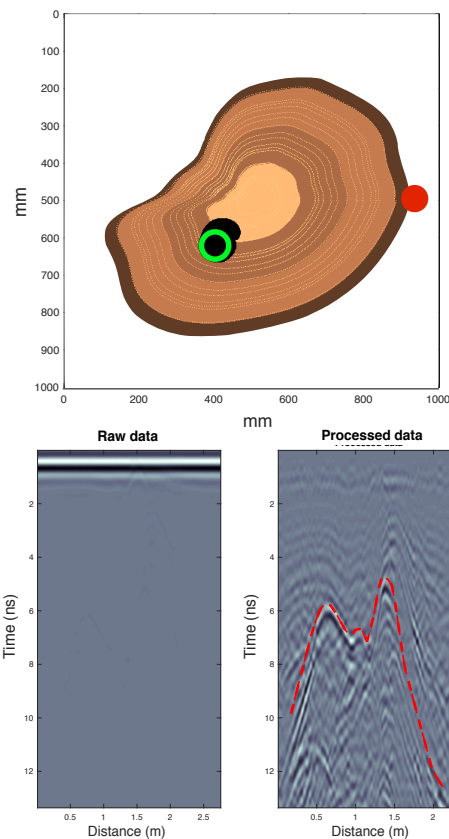


Fig. 4. A complex-shaped hardwood is numerically simulated. Green color illustrates the recovered position and radius of the tree decay. The starting measuring point is highlighted with red circle. The measurements are taken clockwise.

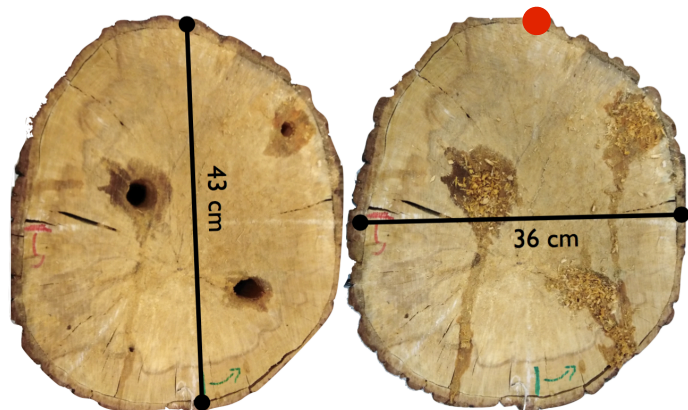


Fig. 5. Left: The tree sample used in the current case study. Right: Sawdust mixed with water used to fill the holes in order to simulate the liquid-filled chambers in early stages of AOD. Red circle illustrates the starting point of the measurements. The measurements are taken counterclockwise.

be constrained to be zero in order to avoid non-uniqueness [28].

The second case study examines how the proposed scheme performs in complex-shaped tree trunks like the one shown in Fig. 4. A complex-shaped hardwood is examined with bark, cambium layer, outer sapwood, inner sapwood and heartwood. **Notice that the complex shape of the trunk does not allow the**

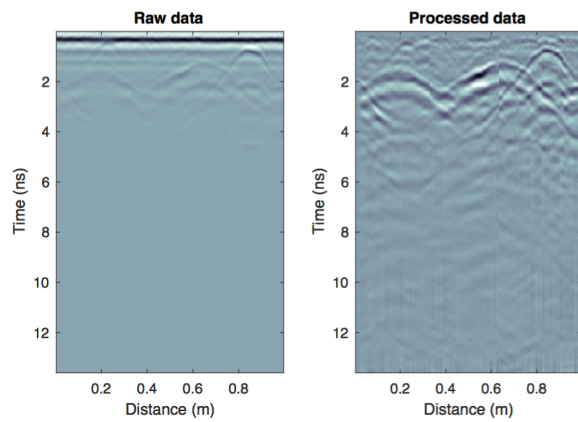


Fig. 6. Left: The raw data collected using Aladdin with perpendicular polarization on the tree sample shown in Fig. 5. Right: The post-processed B-Scan.

tree to be rotated subject to a fixed antenna position. Due to that, the excitation source chosen for this case study is an ideal Hertzian dipole using a modulated Gaussian pulse with 1.5 GHz central frequency. Similar to the previous example, an SVD filter is applied to remove the ringing noise. The bulk relative permittivity is constrained to be equal to  $\epsilon = 14$ . The reflection patterns in the post-processed B-Scan are highly complicated and deviate from the typical hyperbolic features expected in GPR surveys. Patterns like these are difficult to be interpreted and can give the false impression of apparent layers or complex-shaped targets. The proposed methodology manages to accurately recover both the position as well as the size of the decay by fitting the anomaly subject to the shape of the tree trunk.

## V. CASE STUDY

The suggested scheme is now applied to real data collected at the Faringdon center at the University of West London. The investigated tree is the Quercus (oak), which is one of the most common tree species in Europe [66], [67]. Tree diseases are usually slow-progressing agents that gradually compromise the structure and the overall health of trees [68], [69]. Nonetheless, acute oak decline (AOD), a bacterial infection that affects oaks, leads to tree-mortality within few years [68], [69]. Incidents of AOD are increasing globally and AOD is now considered as a serious threat for the oak forests in Europe [68], [69], [70]. The early symptoms of AOD are small liquid-filled chambers within the tree trunk. The latter often reach the outer bark which leads to a characteristic "bleeding" of the tree [68], [69].

In the current case study, the ability of the proposed scheme to detect AOD is tested under laboratory conditions. The host material is a dead oak with three drilled holes with different sizes. One hole with 2 cm radius and two holes with 4 cm radius. The gaps were subsequently filled with sawdust mixed with water in an effort to simulate the liquid-filled cavities that occur in AOD infected oaks (see Fig. 5). The antenna system used is the Aladdin hand-held dual-polarized antenna from IDS Georadar. Aladdin has been successfully applied in many high-frequency GPR applications [71], [72] and its size is



Fig. 7. The estimated coordinates and radii of the decays using the proposed detection scheme are illustrated with green circles. The holes in the tree were filled with saturated sawdust during the measurements (see Fig. 5). The holes are plotted empty in the current figure for comparison purposes.

suitable for measuring curved surfaces such as tree-trunks. The measurements are taken counterclockwise every 1 cm using a measuring wheel. Using the approach described in II.A, the distance is transformed to coordinates. Zero-time removal, time-varying gain and DC-removal are initially applied to the raw data. Subsequently, an SVD and linear filter are used in an effort to reduce the ringing noise present in the B-Scan. In particular, two dominant eigenvalues are filtered out prior to linear filtering. The latter, uses three randomly selected A-Scans to form the  $J$  matrix in (15).

Figure 6 shows both the raw and the processed B-Scans using a perpendicular polarization. Three hyperbolic-features are clearly visible from the post-processed B-Scans. In order to estimate the position/size of the decay that best fits these features, the relative permittivity of the host material should be evaluated first. The bulk relative permittivity of the tree trunk was estimated  $\epsilon \approx 3$  by measuring the two-way travel time from the opposite side of the trunk. A PEC sheet was used in order to further enhance the reflection.

Figure 7 shows the recovered coordinates and radii using the proposed fitting scheme. Three distinct and clearly visible patterns in the B-Scans were manually picked. Based on the shape of the tree and its mean relative permittivity, the minimization in (17) converged to three targets that best fit the data (see Fig. 8). It is evident from Fig. 7, that using the suggested methodology, the positions as well as the radii of the decays can be successfully recovered in an efficient manner.

## VI. CONCLUSIONS

A novel processing framework is described that can be applied to GPR surveys for assessing the internal structure of tree

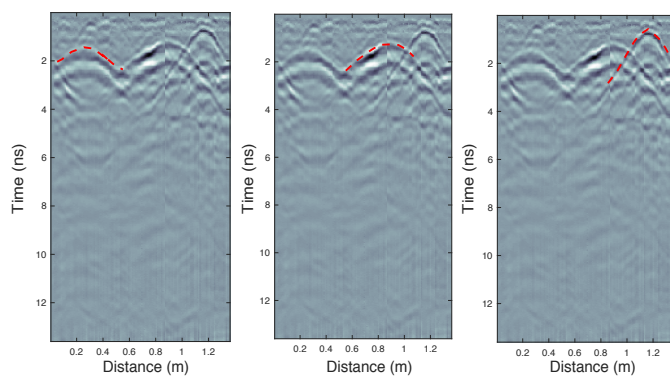


Fig. 8. Three different anomalies used to recover the coordinates and radii of the decays shown in Fig. 7.

trunks. The proposed method can be coupled with commercial antennas with minimum computational and operational requirements. Numerical examples are provided to support the premise that tree decays can be successfully located using typical GPR surveys and thus avoiding tomographic approaches that require custom-made bespoke systems to be deployed on the site of interest. In addition, an experimental case study is presented in which the current scheme is successfully used to locate liquid-filled chambers associated with acute oak decline (AOD). The accuracy and the efficiency of the current methodology on detecting early signs of AOD, makes it commercially appealing for applications such as assessing the health status of trees on forestry applications.

#### ACKNOWLEDGMENT

We thank the Lord Faringdon Charitable Trust for supporting this project. This paper is dedicated to the memory of Jonathon West, a friend, a colleague, a forester, a conservationist and an environmentalist who died following an accident in the woodland that he loved.

#### REFERENCES

- [1] P. Niemz and D. Mannes, "Non-destructive testing of wood and wood-based materials," *J. Cult. Heritage*, vol. 13, pp. S26-S34, 2012.
- [2] V. Bucur, *Nondestructive Characterization and Imaging of Wood*. Berlin, Germany: Springer, 2003.
- [3] H. Lorenzo, V. Prez-Gracia, A. Novo and J. Armesto, "Forestry applications of ground-penetrating radar," *Forest Systems*, vol. 19, pp. 5–17, 2010.
- [4] J. Jezova, L. Mertens and S. Lambot, "Ground-penetrating radar for observing tree trunks and other cylindrical objects," *Construction and Building Materials*, vol. 123, pp. 214–225, 2016.
- [5] R. Pellerin and R. Ross, *Non destructive Evaluation of Wood*, Forest Prod.Society, Madison, Wisconsin, USA, 2002.
- [6] F. Rinn and F. H. Schweingruber, "RESISTOGRAPH and X-ray density charts of wood comparative evaluation of drill resistance profiles and X-ray density charts of different wood species," *Holzforschung*, vol. 50, pp. 303311, 1996.
- [7] L. Costello and S. Quarles, "Detection of wood decay in blue gum and elm: An evaluation of the Resistograph and the portable drill," *Journal of Arboriculture*, vol. 25, pp. 311–317, 1999.
- [8] S. A., Hagrey, "Electrical resistivity imaging of tree trunks," *Near Surface Geophysics*, vol. 4, pp. 179–187, 2006.
- [9] G. Deflorio, S. Fink, and F. W. Schwarze, "Detection of incipient decay in tree stems with sonic tomography after wounding and fungal inoculation," *Wood Science and Technology*, vol. 42, pp. 117–132, 2008.
- [10] A. Catena, "Thermography shows damaged tissue and cavities present in trees," *Nondestructive Characterization of Materials*, vol. 11, pp. 515–522.
- [11] A. Catena, "Thermography reveals hidden tree decay," *Arboricultural Journal* vol. 27, pp. 27–42, 2003.
- [12] A. Catena, and A. G. Catena, "Overview of thermal imaging for tree assessment," *Arboricultural Journal*, vol. 30, pp. 259–270, 2008.
- [13] Q. Wei, B. Leblon, and L. A. Rocque, "On the use of X-ray computed tomography for determining wood properties: a review," *Can. J. For. Res.* vol. 41, pp. 2120–2140, 2001.
- [14] D. Mannes, P. Cherubini, E. Lehmann and P. Niemz, "Neutron imaging versus standard X-ray densitometry as method to measure tree-ring wood density," *Trees Struct. Funct.* vol. 21, pp. 605–612, 2007.
- [15] D. Mannes, *Non-destructive testing of wood by means of neutron imaging in comparison with similar methods*, PhD thesis submitted at ETH Zurich, Switzerland, 2009.
- [16] K. Takahashi and K. Aoiike, "GPR Measurements for Diagnosing Tree Trunk," in *Proc. of 17th International Conference on Ground Penetrating Radar (GPR)*, Rapperswil, 2018, pp. 1-4.
- [17] M. Pastorino, *Microwave Imaging*, Hoboken N.J. John Wiley, 2010.
- [18] L. Fu, S. Liu and L. Liu, "Internal structure characterization of living tree trunk cross-section using GPR: Numerical examples and field data analysis," in *Proc. of the 15th International Conference on Ground Penetrating Radar*, Brussels, 2014, pp. 155-160.
- [19] F. Boero, A. Fedeli, M. Lanini, M. Maffongelli, R. Monleone, M. Pastorino, A. Randazzo, A. Silvade and A. Sansalone, "Microwave Tomography for the Inspection of Wood Materials: Imaging System and Experimental Results," *IEEE Transactions on Microwave Theory and Techniques*, vol. 66, no. 7, pp. 3497-3510, July 2018.
- [20] Z. Miao and P. Kosmas, "Multiple-frequency DBIM-TwIST algorithm for microwave breast imaging," *IEEE Trans. Antennas Propag.*, vol. 65, no. 5, pp. 2507-2516, May 2017.
- [21] C. Gilmore, A. Abubakar, W. Hu, T. M. Habashy, and P. M. V. D. Berg, "Microwave biomedical data inversion using the finite-difference contrast source inversion method," *IEEE Trans. Antennas Propag.*, vol. 57, no. 5, pp. 1528-1538, May 2009.
- [22] A. Klotzsche, J. Van der Kruk, G. A. Meles, and H. Vereecken, "Cross-hole GPR full-waveform inversion of waveguides acting as preferential flow paths within aquifer systems," *Geophysics*, vol. 77, no. 4, pp. H57H62, 2012.
- [23] F. A. Belina, J. Irving, J. R. Ernst, and K. Holliger, "Waveform inversion of crosshole georadar data: Influence of source wavelet variability and the suitability of a single wavelet assumption," *IEEE Trans. Geosci. Remote Sens.*, vol. 50, no. 11, pp. 4610-4625, 2012.
- [24] S. Busch, J. van der Kruk, and H. Vereecken, "Improved characterization of fine-texture soils using on-ground GPR full-waveform inversion," *IEEE Trans. Geosci. Remote Sens.*, vol. 52, no. 7, pp. 3947-3958, Jul. 2014.
- [25] I. Giannakis, A. Giannopoulos and C. Warren, "Realistic FDTD GPR Antenna Models Optimized Using a Novel Linear/Nonlinear Full-Waveform Inversion," *IEEE Trans. on Geoscience and Remote Sensing*, Early Access, 2018.
- [26] D. J. Daniels, *Ground Penetrating Radar*, 2nd ed. London, U.K.: Institution of Engineering and Technology, 2004.
- [27] S. J. Ahn, W. Rauh, H. J. Warnecke, "Least-squares orthogonal distances fitting of circle, sphere, ellipse, hyperbola, and parabola," *Pattern Recognition*, vol. 34, pp. 2283–2303, 2001.
- [28] L. Mertens, R. Persico, L. Matera and S. Lambot, "Automated Detection of Reflection Hyperbolas in Complex GPR Images With No A Priori Knowledge on the Medium," *IEEE Transactions on Geoscience and Remote Sensing*, vol. 54, no. 1, pp. 580–596, Jan. 2016.
- [29] Q. Dou, L. Wei, D. R. Magee and A. G. Cohn, "Real-Time Hyperbola Recognition and Fitting in GPR Data," *IEEE Transactions on Geoscience and Remote Sensing*, vol. 55, no. 1, pp. 51–62, Jan. 2017.
- [30] L. Capineri, P. Grande, and J. A. G. Temple, "Advanced image-processing technique for real-time interpretation of ground-penetrating radar images," *Int. J. Imaging Syst. Technol.*, vol. 9, no. 1, pp. 5159, 1998.
- [31] C. G. Windsor, L. Capineri, and P. Falorni, "A data pair-labeled generalized Hough transform for radar location of buried objects," *IEEE Geosci. Remote Sens. Lett.*, vol. 11, no. 1, pp. 124-127, Jan. 2014.
- [32] W. Alnuaimy, Y. Huang, M. Nakhkash, M. Fang, V. Nguyen, and A. Erisken, "Automatic detection of buried utilities and solid objects with GPR using neural networks and pattern recognition," *J. Appl. Geogr.* vol. 43, pp. 157-165, 2000.
- [33] C. Maas and J. Schmalzl, "Using pattern recognition to automatically localize reflection hyperbolas in data from ground penetrating radar," *Computers & Geosciences*, vo. 58, pp. 116–125, 2013.



- [34] P. Viola and M. J. Jones, "Robust real-time face detection," *Int. J. Comput. Vis.*, vol. 57, no. 2, pp. 137-154, 2004.
- [35] T. Russel and C. Cutler, *Trees, an illustrated identifier and encyclopedia*, Hermes House, Leicestershire, 2012.
- [36] H. Kim, S. J. Cho, and M. J. Yi, "Removal of ringing noise in GPR data by signal processing," *Geosci. J.*, vol. 11, pp. 75-81, Mar. 2007.
- [37] I. Giannakis, S. Xu, P. Aubry, A. Yarovoy and J. Sala, "Signal processing for landmine detection using ground penetrating radar," *IEEE International Geoscience and Remote Sensing Symposium (IGARSS)*, 2016, pp. 7442-7445.
- [38] I. Giannakis, A. Giannopoulos, C. Warren and N. Davidson, "Numerical modelling and neural networks for landmine detection using ground penetrating radar," in *Proc. of 8th International Workshop on Advanced Ground Penetrating Radar (IWAGPR)*, pp. 1-4, 2015.
- [39] J. Kennedy and R. C. Eberhart, "Particle swarm optimization," in *Proc. IEEE Int. Conf. Neural Netw.*, Dec. 1995, vol. 4, pp. 1942-1948.
- [40] R. J. Sharpe, R. W. Thorpe, "Numerical Method for Extracting an Arc Length Parameterization from Parametric Curves", *Computer Aided Design*, vol. 12, no. 2, pp. 79-81, March 1982.
- [41] B., Guenter and R. Parent, "Computing the arc length of parametric curves," *IEEE Comp. Graph. Appl.*, vol. 10, no. 3, pp. 72-78, 1990.
- [42] E. Kreyszig, *Advanced Engineering Mathematics*, 8th ed. New York, NY, USA: Wiley, 1999.
- [43] J. Jezova, J. Harou and S. Lambot, "Reflection waveforms occurring in bistatic radar testing of columns and tree trunks," *Construction and Building Materials*, vol. 174, pp. 388-400, 2018.
- [44] N. Bonomo, D. Bullo, A. Villela and A. Osella, "Ground-penetrating radar investigation of the cylindrical pedestal of a monument," *J. Appl. Geophys.*, vol. 113, pp. 1-13, 2015.
- [45] H. Brunzell, "Detection of shallowly buried objects using impulse radar," *IEEE Trans. Geosci. Remote Sens.*, vol. 37, no. 2, pp. 875-886, Mar. 1999.
- [46] R. Wu, A. Clement, J. Li, E. G. Larsson, M. Bradley, J. Habersat, and G. Maksymenko, "Adaptive ground bounce removal," *Electron. Lett.*, vol. 37, no. 20, pp. 1250-1252, Sep. 2001.
- [47] I. Giannakis, *Realistic numerical modelling of ground penetrating radar for landmine detection* Ph.D. thesis submitted at The University of Edinburgh. 2016.
- [48] J. Robinson and Y. Rahmat-Samii, "Particle swarm optimization in electromagnetics," *IEEE Transactions on Antennas and Propagation*, vol. 52, no. 2, pp. 397-407, Feb. 2004.
- [49] D. F. Kelley, T. J. Destan, and R. J. Luebbers, "Debye function expansions of complex permittivity using a hybrid particle swarm-least squares optimisation approach," *IEEE Trans. Antennas Propag.*, vol. 55, no. 7, pp. 1999-2005, Jul. 2007.
- [50] J. L. Fernandez Martinez, E. G. Gonzalo, J. P. Fernandez Alvarez, H. A. Kuzmaa and C. O. Menendez Perez, "PSO: A powerful algorithm to solve geophysical inverse problems: Application to a 1D-DC resistivity case," *Journal of Applied Geophysics*, vol. 71, no. 1, pp. 13-25, 2010.
- [51] A. Taflov and S. C. Hagness, *Computational Electrodynamics, the Finite-Difference Time-Domain Method*, 2nd ed. Norwood, MA, USA: Artech House, 2000.
- [52] C. Warren, A. Giannopoulos, A. Gray, I. Giannakis, A. Patterson, L. Wetter, A. Hamrah, "A CUDA-based GPU engine for gprMax: Open source FDTD electromagnetic simulation software," *Computer Physics Communications*, Early Access, 2018,
- [53] C. Warren, A. Giannopoulos, and I. Giannakis, "gprMax: Open source software to simulate electromagnetic wave propagation for Ground Penetrating Radar," *Comput. Phys. Commun.*, vol. 209, pp. 163170, Dec. 2016.
- [54] T. Douglas, *Effective Dielectric Constants of Foliage Media*, Rome Air Development Center Air Force Systems Command Griffiss Air Force Base, Rome, 1990.
- [55] N. R. Peplinski, F. T. Ulaby, and M. C. Dobson, "Dielectric properties of soils in the 0.31-3-GHz range," *IEEE Trans. Geosci. Remote Sens.*, vol. 33, no. 3, pp. 803-807, May 1995.
- [56] M. G. Broadhurst, "Complex Dielectric Constants and Dissipation Factor of Foliage," *NBS Report no. 9592, NBS project 3110107, US Naval Ordnance Laboratory*, October 1970.
- [57] G. S. Brown, and W. J. Curry, "A Theory and Model for Wave Propagation Through Foliage", *Radio Science*, vol. 17, pp. 1027-1036, 1982.
- [58] W. L. James, "Dielectric Properties of Wood and Hardboard: Variation With Temperature, Frequency, Moisture Content and Grain Orientation," *USDA Forest Service Res. Paper FPL 245, USDA Forest Products Lab., Madison, MI*, 1975.
- [59] R. J. Birchak, C. G. Gardner, E. J. Hipp, and M. J. Victor, "High dielectric constant microwave probes for sensing soil moisture," in *Proc. of the IEEE*, vl. 62, no. 1, pp 93-98, 1974.
- [60] I. Giannakis and A. Giannopoulos, "A novel piecewise linear recursive convolution approach for dispersive media using the finite-difference time-domain method," *IEEE Trans. Antennas Propag.*, vol. 62, no. 5, pp. 2669-2678, May 2014.
- [61] N. Brazeo, R. Marra, L. Goecke and P. Van Wassenae, "Non-destructive assessment of internal decay in three hardwood species of northeastern North America using sonic and electrical impedance tomography," *Forestry* 84:3339.
- [62] A. Guyot, K. T. Ostergaard, M. Lenkopane, J. Fan and D. A. Lockington, "Using electrical resistivity tomography to differentiate sapwood from heartwood: application to conifers," *Tree Physiology*, vol. 33, no. 2, pp. 187-194, 2013.
- [63] W. C. Shortle, K. R. Dudzik, *Wood Decay in Living and Dead Trees: A Pictorial Overview*, U.S. FOREST SERVICE, 2012.
- [64] B. Larsson, B. A. Bengtsson and M. Gustafsson, *Non Destructive Detection of Decay in Living Trees*, Technical Report LUTEDX/(TEAT-7111)/1-15/(2002); vol. TEAT-7111, 2002.
- [65] C. Warren and A. Giannopoulos, "Creating finite-difference time-domain models of commercial ground-penetrating radar antennas using Taguchi optimisation method," *Geophysics*, vol. 76, no. 2, pp. G37-G47, Apr. 2011.
- [66] C. Humphries, B. Press and D. Sutton, *Guide to Trees of Britain and Europe*, Philip's, London, 2006.
- [67] M. Spohn and R. Spohn, *Trees of Britain and Europe*, A % C Black Publishers Ltd, London, 2008.
- [68] N. Brown, *Epidemiology of acute oak decline in Great Britain*, PhD thesis submitted at Imperial College London, 2014.
- [69] N. Brown, D. J.G. Inward, M. Jeger and S. Denman, "A review of *Agrilus biguttatus* in UK forests and its relationship with acute oak decline," *Forestry: An International Journal of Forest Research*, vol. 88, no. 1, pp. 53-63, 2015.
- [70] S. Denman, N. Brown, S. Kirk, M. Jeger and J. Webber, "A description of the symptoms of Acute Oak Decline in Britain and a comparative review on causes of similar disorders on oak in Europe," *Forestry: An International Journal of Forest Research*, vol. 87, no. 4, pp. 535-551, 2014.
- [71] N. Ahmad, M. Wistuba and H. Lorenz, "GPR as a crack detection tool for asphalt pavements: Possibilities and limitations," in *Proc. of the 14th International Conference on Ground Penetrating Radar (GPR)*, Shanghai, 2012, pp. 551-555.
- [72] S. Lameri, F. Lombardi, P. Bestagini, M. Lualdi and S. Tubaro, "Landmine detection from GPR data using convolutional neural networks," in *Proc. of the 25th European Signal Processing Conference (EUSIPCO)*, Kos, 2017, pp. 508-512.



**Iraklis Giannakis** received the bachelors and masters degrees in geophysics from the Aristotle University of Thessaloniki, Thessaloniki, Greece, in 2009 and 2011, respectively, and the Ph.D. degree from The University of Edinburgh, Edinburgh, U.K., through a Project co-funded by the Defence Science and Technology Laboratory, U.K., and the Engineering and Physical Sciences Research Council, U.K. He is currently a Research Fellow with the School of Computing and Engineering, University of West London, London, U.K., where he has been involved

in applications of ground-penetrating radar (GPR) to sustainable management of forestry heritage. His research interests include near-surface geophysics, nondestructive testing, computational electromagnetics, and machine learning. Dr. Giannakis received the Best Paper Award at the 15th International Conference on GPR in 2014, during his Ph.D. degree.



**Fabio Tosti** received his MSc Engineering degree cum laude in Infrastructure and Transportation Engineering at Roma Tre University, Italy, in 2010, where he also received his PhD with Doctorate (excellent rating), in 2014. He is currently an Associate Professor in Ground Penetrating Radar Technology and Deputy Head of The Faringdon Centre The Non-destructive Testing Centre.

Dr Tosti's research interests include the development of new algorithms, methodologies and numerical models for geoscience applications and the non-destructive assessment, repair and maintenance of civil engineering infrastructures. He has over 120 research publication records in international journals, conferences and books and has served as Managing Guest Editor in numerous international journals.

He served as Organizer, Panel Member (Scientific), and Session Chair in several international conferences and held a supervisory role at the international project European Cooperation in Science and Technology TU1208 Action, titled Civil Engineering Applications of Ground Penetrating Radar.

In 2017 Dr Tosti was granted an Early Career Scientists Award by the European Geosciences Union (EGU) for his outstanding contribution to the development of new GPR methodologies in geosciences and civil engineering. Additionally he holds the post of Convener at the EGU General Assembly for sessions on NDT methods and data fusion.



**Livia Lantini** received her BSc (Hons) degree in Civil Engineering and her MSc degree in Infrastructure and Transportation Engineering at the Department of Engineering Roma Tre University, Italy. Since 2018 she is a PhD student at the School of Computing and Engineering of the University of West London. Her research focuses on the assessment and health monitoring of trees and the investigation of tree roots and soil interaction using Ground Penetrating Radar and other non-destructive methods.



**Amir Alani** joined the University of West London, UK, in 2014. In addition to his position as the Executive Dean of the School of Computing and Engineering, he leads the Faringdon Centre (the Non-Destructive Research Centre) at the University.

Professor Alani is an expert in the assessment, repair, and maintenance of civil engineering infrastructures such as bridges, tunnels, and buildings and has extensive work experience with different professional bodies in the fields of engineering and design both in the UK and Europe. He was appointed as the Rochester Bridge Trust Professor of Engineering in 2018 and has more than 25 years work experience in Higher Education and industry in the UK.

With an established track record of research and development in different branches of civil and mechanical engineering, including the applications of non-destructive testing methods, concrete technology, geotechnics and soil engineering and engineering education, Professor Alani has published over 180 journal papers, book chapters, international conference papers, and consulting external reports in these areas.

Professor Alani was a Management Committee Member for a European Cooperation in Science and Technology (COST) Action project, TU1208 Project 2012-2017, Civil Engineering Applications of Ground Penetrating Radar (GPR). He has delivered and led numerous seminars and workshops nationally and internationally, and has chaired a number of international conference sessions in the last 20 years.